NANO LETTERS

Letter

pubs.acs.org/NanoLett

Multipositional Silica-Coated Silver Nanoparticles for High-Performance Polymer Solar Cells

Hyosung Choi,[†] Jung-Pil Lee,[†] Seo-Jin Ko,[†] Jae-Woo Jung,[‡] Hyungmin Park,[†] Seungmin Yoo,[†] Okji Park,[†] Jong-Ryul Jeong,[‡] Soojin Park,*[,†] and Jin Young Kim*[,†]

[†]Interdisciplinary School of Green Energy and KIER-UNIST Advanced Center for Energy, Ulsan National Institute of Science and Technology (UNIST), Ulsan, 689-798, South Korea

[‡]Department of Materials Science and Engineering, Graduate School of Green Energy Technology, Chungnam National University, Daejeon 305-764, South Korea

Supporting Information

ABSTRACT: We demonstrate high-performance polymer solar cells using the plasmonic effect of multipositional silica-coated silver nanoparticles. The location of the nanoparticles is critical for increasing light absorption and scattering via enhanced electric field distribution. The device incorporating nanoparticles between the hole transport layer and the active layer achieves a power conversion efficiency of 8.92% with an external quantum efficiency of 81.5%. These device efficiencies are the highest values reported to date for plasmonic polymer solar cells using metal nanoparticles.

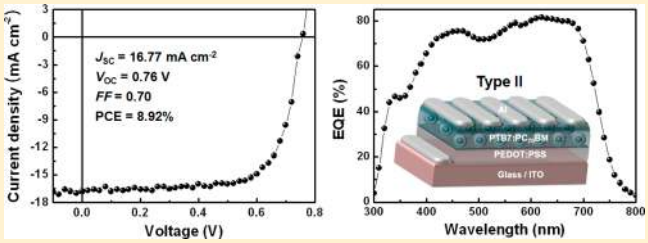

KEYWORDS: *Surface plasmon resonance, polymer solar cells, metal nanoparticles, light absorption, electric field distribution*

Polymer solar cells (PSCs) have attracted a lot of interest due to their many advantages, including low cost, solution processability, and mechanical flexibility.[1−5] Although the intensive development of new materials and device architectures has improved power conversion efficiencies (PCE) up to 8% in single-junction bulk heterojunction (BHJ) PSCs,[6−11] further improvement is still necessary for commercialization. Strategies to maximize photovoltaic parameters, including short-circuit current density (J_{SC}), open-circuit voltage (V_{OC}), and fill factor (FF), have included bandgap engineering of conjugated polymers,[6,9−11] introduction of buffer layers,[2,12,13] and morphology control using processing additives or post fabrication treatments, and so forth.[14−17] Among many strategies for improving J_{SC}, one simple approach is to increase light absorption in the active layer using thick BHJ films. However, the thickness of the active layer is limited by the low carrier mobilities of BHJ materials.[2,18−20] Therefore, it is necessary to find ways to minimize the thickness of BHJ films while maximizing the light absorption capability in the active layer.

The surface plasmon resonance (SPR) effect of metal nanoparticles (NPs) can be an effective way to store incident light energy in localized surface plasmon modes and enhance the photogeneration of excitons.[21,22] Excitation of surface plasmons by light at specific wavelengths at which resonance occurs can result in strong light-scattering with the appearance of intense surface plasmon absorption bands and an enhancement of local electromagnetic fields.[23,24] There have been many reports on the SPR effect not only that incorporate metal NPs into the hole transport layer (HTL),[25−27] active layer,[18,19,28,29] or at the anode/HTL interface,[20,30,31] but also that utilize two different metal NPs or combinations of metal NPs and metal nanograting electrodes.[27,32]

To maximize the SPR effect on device performance, it is essential to control the distance between metal NPs and the active layer. When the distance is too close, exciton quenching occurs by nonradiative energy transfer.[18,19,30] However, the interaction between surface plasmons and excitons exponentially decreases as the distance between metal NPs and the active layer increases.[33] Therefore, metal NPs have been introduced at the interface of indium tin oxide (ITO) and poly(3,4-ethylenedioxythiophene):polystyrene sulfonic acid (PEDOT:PSS) or embedded in PEDOT:PSS layer. To date, there have been no reports in which metal NPs have been introduced between the PEDOT:PSS and active layers. In spite of a few successful reports on direct mixing of metal NPs in the active layer,[18,19,29] there is always a concern about poor device performance caused by exciton quenching. Furthermore, it is difficult to uniformly disperse metal NPs within the active layer while maintaining control of the morphology.

Here, we report high-performance PSCs employing the SPR effect via multipositional silica-coated silver NPs (Ag@SiO_2). The silica shell in Ag@SiO_2 preserves the SPR effect of the Ag NPs by preventing oxidation of the Ag core under ambient conditions and also eliminates the concern about exciton

Received: February 26, 2013
Revised: April 19, 2013
Published: April 22, 2013

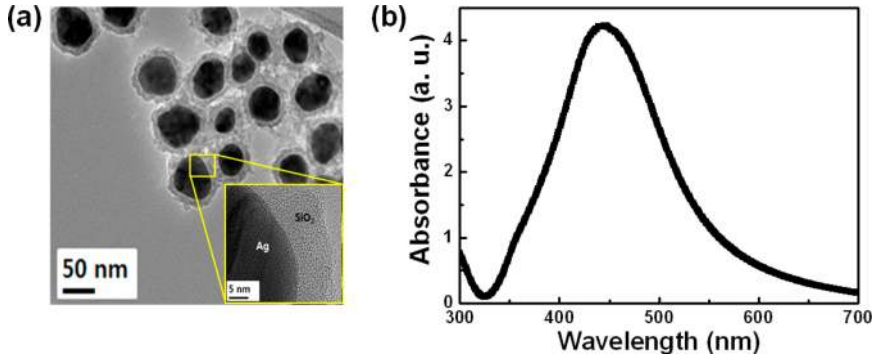

Figure 1. (a) HR-TEM image and (b) UV−vis absorption spectrum of Ag@SiO_2. The inset of part a shows a magnification of the SiO_2 layer, which has an average thickness of 10 nm.

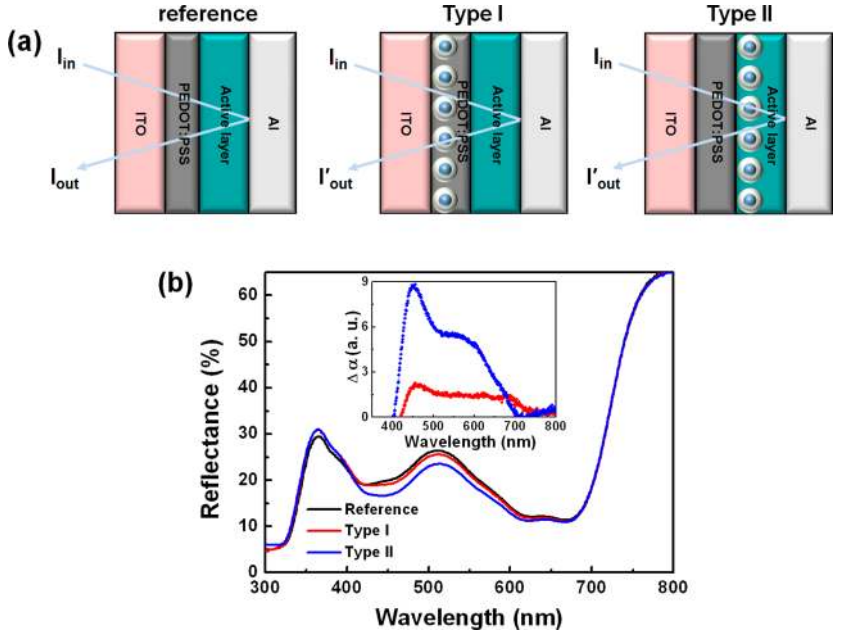

Figure 2. (a) Device structures and (b) reflectance spectra of PTB7:$PC_{70}BM$-based PSCs with different spatial locations of Ag@SiO_2. The inset shows the absorption enhancement ($\Delta\alpha$) caused by Ag@SiO_2.

quenching by avoiding direct contact between Ag cores and the active layer. The multipositional property refers to the ability of Ag@SiO_2 NPs to be introduced at both ITO/PEDOT:PSS (type I) and PEDOT:PSS/active layer (type II) interfaces in polymer:fullerene-based BHJ PSCs due to the silica shells. The type II structure shows strong light absorption and scattering via enhanced electric field distribution compared to the type I structure, resulting in remarkable enhancement in J_{SC} and thus PCE.

Results and Discussion. Silver nanoparticles (Ag NPs) were prepared by the polyol reduction of silver nitrate with ethylene glycol at a high temperature in the presence of poly(vinyl pyrrolidone) (PVP). The use of PVP allowed Ag NPs with uniform size and shape to be synthesized and stably dispersed in solution. The PVP covered Ag NPs with were then encapsulated with silica via a sol−gel process. Figure 1a shows a high-resolution transmission electron microscopy (HR-TEM) image of Ag@SiO_2 NPs. It can clearly be seen that the Ag@SiO_2 NPs were successfully synthesized with a well-defined core−shell structure.

As-prepared Ag NPs were spherical and had relatively uniform diameters of about 50 nm. The silica shell uniformly and completely coated the surface of the individual Ag NPs with an average thickness of 10 nm. For clarity, a magnified TEM image of Ag NPs is shown in the inset of Figure 1a. The distinct boundary between Ag NPs and silica is clearly visible due to a large difference in electron density between the crystalline Ag core and the amorphous silica shell. Uniform films of Ag@SiO_2 NPs could be formed on silicon substrates via spin-coating, confirmed by scanning electron microscope (Figure S1), demonstrating the well-dispersed behavior of the NPs. Figure 1b shows the UV−vis absorption spectrum of an Ag@SiO_2 solution dispersed in ethanol. Compared to bare Ag NPs with the same size (about 50 nm), Ag@SiO_2 NPs exhibit a red-shifted SPR peak at 450 nm, caused by the silica shell (Figure S2). This implies that the SPR peak can be tuned by engineering the dielectric constant of the surrounding matrix.[21,34] To investigate changes in absorption, we performed reflectance measurements using two device configurations, as shown in Figure 2a. For the active layers, we used a blend solution of poly[[4,8-bis[(2-ethylhexyl)oxy]benzo[1,2-b:4,5-b′]dithiophene-2,6-diyl][3-fluoro-2-[(2-ethylhexyl)-carbonyl]-thieno-[3,4-*b*]thiophenediyl]] (PTB7) as an electron donor and [6,6]-phenyl-C_{70} butyric acid methyl ester ($PC_{70}BM$) as an

dx.doi.org/10.1021/nl400730z | *Nano Lett.* 2013, 13, 2204−2208

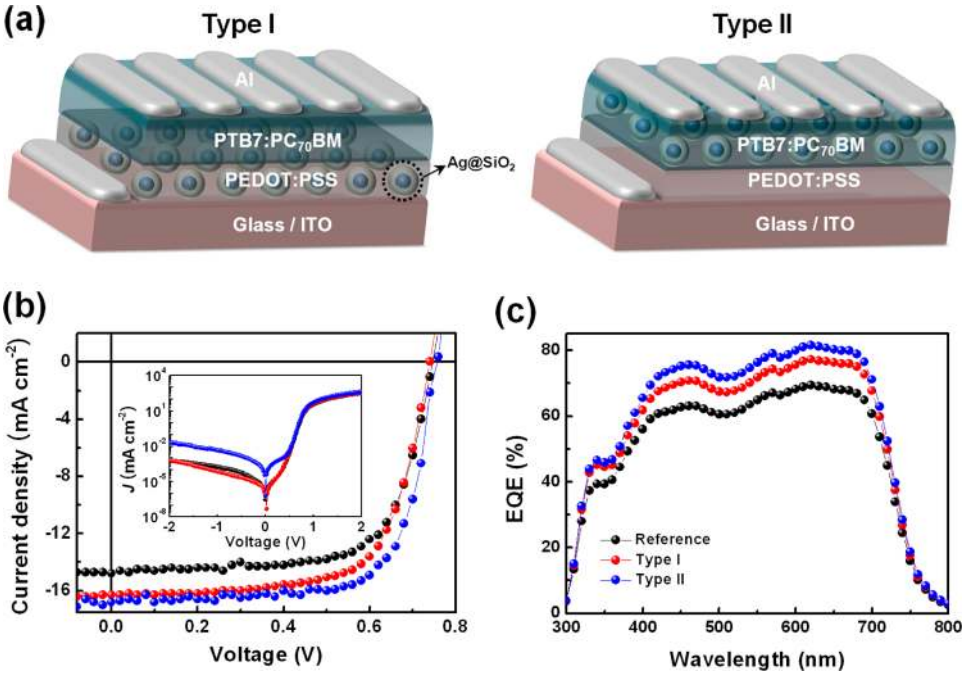

Figure 3. (a) Device structures, (b) $J-V$ characteristics, and (c) EQE of PTB7:$PC_{70}BM$-based PSCs with type I and type II architectures. Type I: ITO/Ag@SiO_2/PEDOT:PSS/PTB7:$PC_{70}BM$/Al, and type II: ITO/PEDOT:PSS/Ag@SiO_2/PTB7:$PC_{70}BM$/Al.

Table 1. Device Characteristics of PTB7:$PC_{70}BM$-Based PSCs with Different Ag@SiO_2 Locations

device configuration	J_{SC} (mA/cm^2)	V_{OC} (V)	FF	average PCE (%)	best PCE (%)	J_{SC} (Calc.) (mA/cm^2)
reference	14.64 ± 0.14	0.74 ± 0.01	0.67 ± 0.01	7.26	7.51	14.55
Type I	16.10 ± 0.21	0.74 ± 0.01	0.67 ± 0.01	7.98	8.20	16.19
Type II	16.65 ± 0.12	0.74 ± 0.02	0.68 ± 0.02	8.49	8.92	17.14

electron acceptor. Two structures were used; type I and II consisting of ITO/Ag@SiO_2/PEDOT:PSS/PTB7:$PC_{70}BM$/Al and ITO/PEDOT:PSS/Ag@SiO_2/PTB7:$PC_{70}BM$/Al, respectively. A device without Ag@SiO_2 was used as a reference. Due to the insolubility of PEDOT:PSS in ethanol, the Ag@SiO_2 solution can be directly spin-coated on top of PEDOT:PSS layer without removing the underlying PEDOT:PSS. Reflectance measurements were carried out to elucidate total light absorption using different device architectures. Figure 2b shows reflectance spectra of PTB7:$PC_{70}BM$-based PSCs with type I and type II architectures, compared to the structure without Ag@SiO_2.

The type II device exhibits greater light absorption than type I in the range of 400−700 nm, showing a noticeable SPR peak at 450 nm, which is in good agreement with UV−vis absorption spectrum of the Ag@SiO_2 solution.

To investigate the effect of different spatial locations of Ag@SiO_2 NPs on light absorption, we calculated absorption enhancement ($\Delta\alpha$) from reflectance measurements based on following equation,[2]

$$\alpha(x) = -\left(\frac{1}{2}d\right)\ln\left[\frac{I'_{out}(x)}{I_{out}(x)}\right] \quad (1)$$

where d is the thickness of active layer, I_{out} is the intensity of the reflected light from the device without Ag@SiO_2, and I'_{out} is the intensity of the reflected light from the device with Ag@SiO_2. Although we used same concentration and spin-coating condition for depositing Ag@SiO_2, type II showed a 4-fold increase in light absorption at the SPR peak of 450 nm and a broader absorption band ranging from 400 to 700 nm, compared to the device with type I architecture (inset, Figure 2b). These results are in good agreement with simulated electric field distributions and extinction spectra of Ag@SiO_2 with different surrounding matrices (Figure S3).

Based on the plasmonic effect of Ag@SiO_2 at both ITO/PEDOT:PSS (type I) and PEDOT:PSS/active layer (type II) interfaces, we fabricated PTB7:$PC_{70}BM$-based PSCs to evaluate the ability of Ag@SiO_2 to enhance device performance, as shown in Figure 3a. The device without Ag@SiO_2 is used as the reference. Figure 3b and c shows current density versus voltage ($J-V$) characteristics and external quantum efficiency (EQE) of the devices without Ag@SiO_2 and with type I and II structures. Detailed device parameters are listed in Table 1. More than 150 devices were fabricated to optimize the device efficiency by controlling the concentration of Ag@SiO_2 in PTB7:$PC_{70}BM$-based PSCs with type I and II (Figure S4 and Table S1). The best reference device had a short-circuit current density (J_{SC}) of 14.80 mA cm^{-1}, an open-circuit voltage (V_{OC}) of 0.75 V, a fill factor (FF) of 0.68, and PCE of 7.51%. These device characteristics are comparable to other reports using PTB7:$PC_{70}BM$ blend films as the active layer.[8,27] For the device with type I architecture, we obtained an improved PCE of 8.20%, resulting from an enhancement in J_{SC} (16.31 mA cm^{-1}). Surprisingly, the device with type II architecture exhibited an even greater improvement in J_{SC} (16.77 mA cm^{-1}), leading to a higher PCE of 8.92%. To the best of our knowledge, this PCE is the highest value reported to date in plasmonic PSCs using metal NPs (Table S2). The optimized devices with type I and II architectures show ∼10% and ∼19%

dx.doi.org/10.1021/nl400730z | Nano Lett. 2013, 13, 2204−2208

increase in the PCE values, respectively, compared to that of reference device. The highest PCE from type II is attributed to a stronger coupling effect due to the close distance between the Ag NPs and the active layer (Figure S3a). It is important to note that the type II device architecture is possible because the silica shell prevents exciton quenching and charge recombination which would occur if there was direct contact between Ag NPs and the active layer.

The inset of Figure 3b shows the effect of $Ag@SiO_2$ location on dark *J-V* characteristics. The three types of device exhibit negligible differences in dark *J*−*V* characteristics, implying no significant influence of $Ag@SiO_2$ NPs on charge transport characteristics. This is also confirmed by the work function of the PEDOT:PSS films as measured by ultraviolet photoemission spectroscopy, which remains constant regardless of the presence of $Ag@SiO_2$ (Figure S5). These improvements in PCE using $Ag@SiO_2$ originate from increases in J_{SC}, which are consistent with EQE enhancement, as shown in Figure 3c, whereas V_{OC} and FF remain almost constant. The device without $Ag@SiO_2$ exhibits a maximum EQE of 69.4%, while devices with type I and type II architectures exhibit enhanced EQEs of 77.3% and 81.5%, respectively. High and broad EQE enhancements ranging from 400 to 700 nm result from the combination of light absorption and scattering caused by $Ag@SiO_2$ NPs. Additional light absorption from 400 to 600 nm contributes to improvements in EQE in this spectral region, while EQE enhancement in the range of 600−700 nm may also be attributed to light scattering by $Ag@SiO_2$ NPs, which render the surface of the active layer rougher (Table S3 and Figure S6) and increase the effective path length of light penetrating into the polymer matrix.

To investigate the relationships among EQE enhancement (ΔEQE), absorption change (Δabsorption), and $Ag@SiO_2$ location, we calculated the absorption (A) from total reflection (R) and transmission (T) using $A = 1 - R - T$,[32] and calculated the EQE difference by subtracting the EQE of the device without $Ag@SiO_2$ from that of the device with $Ag@SiO_2$. Because metal deposited on the active layer is considered a perfect mirror, we ignored transmission in real devices. The difference in EQE enhancement by $Ag@SiO_2$ NPs in type I and II architectures correlates well with absorption enhancement in both cases (Figure S6).

To compare the effect of $Ag@SiO_2$ and bare Ag NPs on device performance, PTB7:PC_{70}BM-based PSCs were fabricated in which $Ag@SiO_2$ NPs were replaced with bare Ag NPs in both type I and II device architectures. The type I devices with bare Ag NPs showed a 10% enhancement in J_{SC} and PCE (Figure S7a and Table S4). This enhancement originates from additional light absorption by Ag NPs but not from light scattering effects (Figure S8). Although additional light absorption contributed to EQE enhancement ranging from 350 to 550 nm in type II devices with bare Ag NPs, we observed poor device performance, likely caused by exciton quenching from direct contact between Ag NPs and the active layer (Figure S7b). This result confirms that the silica shells are critical to the successful utilization of plasmonic NPs in type II architectures, where they prevent exciton quenching while enabling light absorption and scattering effects for enhanced device performance.

In summary, we demonstrate high-performance PSCs using multipositional $Ag@SiO_2$ NPs as plasmonic materials. The change of $Ag@SiO_2$ location leads to different surrounding matrices for $Ag@SiO_2$ and enhancement of electric field distribution, giving rise to significant differences in light absorption and scattering. The incorporation of $Ag@SiO_2$ into the PTB7:PC_{70}BM-based PSCs remarkably improves device performance in both type I and II structures. Particularly, the type II structure employing $Ag@SiO_2$ at the PEDOT:PSS/active layer interface resulted in a PCE of 8.92% and EQE of 81.5% via additional light absorption and scattering effects over a broad spectral range of 400−700 nm. These device efficiencies are the highest values reported to date for plasmonic PSCs using metal nanoparticles. Furthermore, this is the first report introducing metal NPs between the hole transport layer and active layer for enhancing device performance. The multipositional and solution-processable properties of our SPR materials offer the possibility to use multiple plasmonic effects by introducing various metal nanoparticles into different spatial locations for high-performance optoelectronic devices via mass production techniques.

■ ASSOCIATED CONTENT

Ⓢ Supporting Information

A detailed description of the synthetic procedures and device fabrication, as well as SEM image, AFM images, absorption spectra, photoelectron spectra, additional *J*−*V* characteristics, and tables. This material is available free of charge via the Internet at http://pubs.acs.org.

■ AUTHOR INFORMATION

Corresponding Author

*E-mail: jykim@unist.ac.kr (J. Y. Kim); spark@unist.ac.kr (S. Park).

Author Contributions

H.C. and J.-P.L. contributed equally to this work.

Notes

The authors declare no competing financial interest.

■ ACKNOWLEDGMENTS

This research was supported by WCU (World Class University) program through the Korea Science and Engineering Foundation funded by the Ministry of Education, Science and Technology (R31-2008-000-20012-0), the National Research Foundation of Korea Grant (2009-0093020), and the International Cooperation of the Korea Institute of Energy Technology Evaluation and Planning (KETEP) grant funded by the Korea government Ministry of Knowledge Economy (2012T100100740).

■ REFERENCES

(1) Yu, G.; Gao, J.; Hummelen, J. C.; Wudl, F.; Heeger, A. J. *Science* **1995**, *270*, 1789−1791.
(2) Kim, J. Y.; Kim, S. H.; Lee, H. H.; Lee, K.; Ma, W.; Gong, X.; Heeger, A. J. *Adv. Mater.* **2006**, *18*, 572−576.
(3) Günes, S.; Neugebauer, H.; Sariciftci, N. S. *Chem. Rev.* **2007**, *107*, 1324−1338.
(4) Kim, J. Y.; Lee, K.; Coates, N. E.; Moses, D.; Nguyen, T.-Q.; Dante, M.; Heeger, A. J. *Science* **2007**, *317*, 222−225.
(5) Li, G.; Zhu, R.; Yang, Y. *Nat. Photonics* **2012**, *6*, 153−161.
(6) Son, H. J.; Lu, L.; Chen, W.; Xu, T.; Zheng, T.; Carsten, B.; Strzalka, J.; Darling, S. B.; Chen, L. X.; Yu, L. *Adv. Mater.* **2013**, *25*, 838−843.
(7) Chu, T.-Y.; Lu, J.; Beaupré, S.; Zhang, Y.; Pouliot, J.-R.; Wakim, S.; Zhou, J.; Leclerc, M.; Li, Z.; Ding, J.; Tao, Y. *J. Am. Chem. Soc.* **2011**, *133*, 4250−4253.
(8) Liang, Y.; Xu, Z.; Xia, J.; Tsai, S.-T.; Wu, Y.; Li, G.; Ray, C.; Yu, L. *Adv. Mater.* **2010**, *22*, E135−E138.

(9) Chen, H.-C.; Chen, Y.-H.; Liu, C.-C.; Chien, Y.-C.; Chou, S.-W.; Chou, P.-T. *Chem. Mater.* **2012**, *24*, 4766−4772.
(10) Huang, Y.; Guo, X.; Liu, F.; Huo, L.; Chen, Y.; Russell, T. P.; Han, C. C.; Li, Y.; Hou, J. *Adv. Mater.* **2012**, *24*, 3383−3389.
(11) Dou, L.; Chang, W.-H.; Gao, J.; Chen, C.-C.; You, J.; Yang, Y. *Adv. Mater.* **2013**, *25*, 825−831.
(12) Yuan, Y.; Reece, T. J.; Sharma, P.; Poddar, S.; Ducharme, S.; Gruverman, A.; Yang, Y.; Huang, J. *Nat. Mater.* **2011**, *10*, 296−302.
(13) Steirer, K. X.; Ndione, P. F.; Widjonarko, N. E.; Lloyd, M. T.; Meyer, J.; Ratcliff, E. L.; Kahn, A.; Armstrong, N. R.; Curtis, C. J.; Ginley, D. S.; Berry, J. J.; Olson, D. C. *Adv. Energy Mater.* **2011**, *1*, 813−820.
(14) Lee, J. K.; Ma, W. L.; Brabec, C. J.; Yuen, J.; Moon, J. S.; Kim, J. Y.; Lee, K.; Bazan, G. C.; Heeger, A. J. *J. Am. Chem. Soc.* **2008**, *130*, 3619−3623.
(15) Jo, J.; Kim, S.-S.; Na, S.-I.; Yu, B.-K.; Kim, D.-Y. *Adv. Funct. Mater.* **2009**, *19*, 866−874.
(16) Peet, J.; Kim, J. Y.; Coates, N. E.; Ma, W. L.; Moses, D.; Heeger, A. J.; Bazan, G. C. *Nat. Mater.* **2007**, *6*, 497−500.
(17) Liu, X.; Wen, W.; Bazan, G. C. *Adv. Mater.* **2012**, *24*, 4505−4510.
(18) Wang, D. H.; Park, K. H.; Seo, J. H.; Seifter, J.; Jeon, J. H.; Kim, J. K.; Park, J. H.; Park, O. O.; Heeger, A. J. *Adv. Energy Mater.* **2011**, *1*, 766−770.
(19) Wang, D. H.; Kim, D. Y.; Choi, K. W.; Seo, J. H.; Im, S. H.; Park, J. H.; Park, O. O.; Heeger, A. J. *Angew. Chem., Int. Ed.* **2011**, *50*, 5519−5523.
(20) Heo, M.; Cho, H.; Jung, J.-W.; Jeong, J.-R.; Park, S.; Kim, J. Y. *Adv. Mater.* **2011**, *23*, 5689−5693.
(21) Atwater, H. A.; Polman, A. *Nat. Mater.* **2010**, *9*, 205−213.
(22) Hutter, E.; Fendler, J. H. *Adv. Mater.* **2004**, *16*, 1685−1706.
(23) Kulkarni, A. P.; Noone, K. M.; Munechika, K.; Guyer, S. R.; Ginger, D. S. *Nano Lett.* **2010**, *10*, 1501−1505.
(24) Kumar, A.; Srivastava, R.; Tyagi, P.; Mehta, D. S.; Kamalasanan, M. N. *Org. Electron.* **2012**, *13*, 159−165.
(25) Fung, D. D. S.; Qiao, L.; Choy, W. C. H.; Wang, C.; Sha, W. E. I.; Xie, F.; He, S. *J. Mater. Chem.* **2011**, *21*, 16349−16356.
(26) Chen, F.-C.; Wu, J.-L.; Lee, C.-L.; Hong, Y.; Kuo, C.-H.; Huang, M. H. *Appl. Phys. Lett.* **2009**, *95*, 013305.
(27) Lu, L.; Luo, Z.; Xu, T.; Yu, L. *Nano Lett.* **2013**, *13*, 59−64.
(28) Wang, C. C. D.; Choy, W. C. H.; Duan, C.; Fung, D. D. S.; Sha, W. E. I.; Xie, F.-X.; Huang, F.; Cao, Y. *J. Mater. Chem.* **2012**, *22*, 1206−1211.
(29) Li, X.; Choy, W. C. H.; Lu, H.; Sha, W. E. I.; Ho, A. H. P. *Adv. Funct. Mater.* **2013**, DOI: 10.1002/adfm.201202476.
(30) Kim, S.-S.; Na, S.-I.; Jo, J.; Kim, D.-Y.; Nah, Y.-C. *Appl. Phys. Lett.* **2008**, *93*, 073307.
(31) Morfa, A. J.; Rowlen, K. L.; Reilly, T. H., III; Romero, M. J.; Lagemaat, J. v. d. *Appl. Phys. Lett.* **2008**, *92*, 013504.
(32) Li, X.; Choy, W. C. H.; Huo, L.; Xie, F.; Sha, W. E. I.; Ding, B.; Guo, X.; Li, Y.; Hou, J.; You, J.; Yang, Y. *Adv. Mater.* **2012**, *24*, 3046−3052.
(33) Ostrowski, J. C.; Mikhailovsky, A.; Bussian, D. A.; Summers, M. A.; Buratto, S. K.; Bazan, G. C. *Adv. Funct. Mater.* **2006**, *16*, 1221−1227.
(34) Beck, F. J.; Polman, A.; Catchpole, K. R. *J. Appl. Phys.* **2009**, *105*, 114310.